Chapter 21
Sustainable Energy Harvesting Using Efficient α-Fe_2O_3 Photoanode Through Photocatalytic Water Splitting Using Facile Chemical Route

Avinash Rokade, Vidhika Sharma, Mohit Prasad and Sandesh Jadkar

Abstract Here, a simple, controlled and cost effective electrodeposition technique was used to synthesize α-Fe_2O_3 hematite photo-electrode for solar water splitting. We have synthesized thin films of α-Fe_2O_3 by varying electrodeposition potential from −0.2 to 0 V at optimum conditions of cycles by using potentiostat. The obtained ferrihydrite thin films were transformed into α-Fe_2O_3 thin films by annealing them at 600 °C for 1 h. Films were investigated by XRD, SEM, UV-Visible and Raman spectroscopy for their structural, optical and morphological properties. Further suitability of α-Fe_2O_3 thin films as a photo-electrode has been evaluated by photoelectrochemical (PEC) measurements which exhibited photocurrent density of 65 μA/cm^2 at 0.5 V versus SCE under AM 1.5 100 mW/cm^2 illumination. The effective enhancement in photocurrent conversion efficiency with optimum film thickness has been observed upon light irradiation. The absorption spectrum of the α-Fe_2O_3 shows significant absorption in the visible region. However, photo-conversion efficiency is quite low. The obtained results suggest that the well controlled thick α-Fe_2O_3 material can be utilized as a shell layer with wide band gap nano-structured semiconductor like ZnO, TiO_2 to form hetero-structure for solar water splitting application.

Keywords α-Fe_2O_3 · Photoelectrochemical · XRD · SEM · UV-Visible spectroscopy · Raman spectroscopy

A. Rokade
School of Energy Studies, Savitribai Phule Pune University, Pune 411 007, India

V. Sharma · M. Prasad · S. Jadkar (✉)
Department of Physics, Savitribai Phule Pune University, Pune 411 007, India
e-mail: sandesh@physics.unipune.ac.in

G. Anand et al. (eds.), *Nanotechnology for Energy and Water*,
Springer Proceedings in Energy, https://doi.org/10.1007/978-3-319-63085-4_21

21.1 Introduction

Semiconductor photocatalyst is one of the most promising technologies for conversion of solar energy into hydrogen via water-splitting process for the future fuel is a viable alternative to fossil fuels because large quantity of hydrogen can potentially be generated in a clean and sustainable manner [1]. Fujishima and Honda in 1972 demonstrated the phenomenon of photocatalysis using single crystal TiO_2 as a working electrode [2]. Iron oxide (α-Fe_2O_3) is an important semiconductor which has recently attracted the attention for production of hydrogen via water splitting. It has the ability to absorb a large part of solar spectrum due to its favorable band gap (2.0–2.2 eV) [3, 4]. It is also inexpensive, plentiful, readily available, non toxic, chemically stable in aqueous environment and has good environmental acceptability [5, 6] which favors the fundamental and practical research for its applications in many fields such as Li-ion batteries [7, 8], supercapacitors [9], peroxide sensor [10], solar energy conversion via water splitting [11], dye degradation [12], water purification and treatment [13, 14]. Thus, study of α-Fe_2O_3 thin films for photocatalytic water splitting is a important topic of research in production of hydrogen fuel. The maximum theoretical solar-to-hydrogen (STH) conversion efficiency at standard solar illumination conditions for α-Fe_2O_3 was found $\sim$15% [15, 16].

The α-Fe_2O_3 thin films can be prepared by various methods such as chemical vapor deposition [17], sol-gel process [18], pulsed laser evaporation [19], reactive sputtering [20], hydrothermal technique [15, 21], spray pyrolysis [22, 23] etc. However, for preparation of hematite α-Fe_2O_3 thin films there are certain challenges which need to be overcome such as non-optimal conduction band edge alignment for hydrogen evolution potential and indirect band gap causing low absorption of light. Also it possesses short carrier diffusion length in the range of 2–4 nm [24], 20 nm [25] giving low transport and low conductivity of photo generated carriers [11, 26]. The short diffusion length of holes can be overcome by synthesis of extremely thin films of hematite α-Fe_2O_3 material by controlled deposition technique. With this motivation an attempt has been made to prepare α-Fe_2O_3 thin films of well-defined thickness by simple electrochemical deposition technique. This technique consists of three electrode system with FTO coated glass working substrate, platinum counter electrode and SCE as the reference electrode. In this study we have tried to use thin films of α-Fe_2O_3 as working electrode by controlling thickness of deposition layers using cyclic voltammetry.

21.2 Experimental

The potentiostatic electrochemical deposition were performed by an Metrohm Autolab potentiostat PGSTAT302 N model in three-electrode cell configuration system controlled by a personal computer (PC), working electrode (FTO glass

substrate), reference electrode (SCE) and counter electrode (Pt). The FTO coated glass substrate were ultrasonically cleaned before starting the deposition using acetone, ethanol and distilled water for 5 min each. The chemical solution were prepared using aqueous electrolyte of 0.05 M Ferric Chloride ($FeCl_3$), 0.05 M Potassium Fluoride (KF), 0.1 M Potassium Chloride (KCl) and 1 M Hydrogen Peroxide (H_2O_2). The films of Fe_2O_3 are electrochemically synthesized by 30 deposition cycles from −0.2 to 0 V (scan rate 20 mV/S) at room temperature. The obtained ferrihydrite thin films were transformed into α-Fe_2O_3 thin films by annealing at 600 °C in ambient atmosphere for 1 h. The surface morphology of the films was analysed using a JEOL JSM-6360A scanning electron microscope (SEM) with operating voltage 20 kV. The optical band gap of the films was calculated from absorption spectra and was measured in the range of 200–800 nm using a JASCO, V-670 UV-Visible spectrophotometer. Rein-shaw Raman spectrometer was used to record raman spectra in the range of 100–800 cm^{-1}. Raman spectrum was detected using the spectrometer having backscattering geometry with the resolution of 1 cm^{-1}. The He–Ne laser of 632.8 nm line was used as the excitation source at room temperature. To avoid laser induced crystallization the power of the Raman laser was kept less than 5 mW. X-ray diffractometer (Bruker D8 Advance, Germany) using CuKα line (λ = 1.54 Å) was used to obtain the x-ray diffraction patterns. The photoelectrochemical measurements with a potentiostat (AUTOLAB N302) were carried out in a three electrode configuration by employing a platinum foil as the counter, SCE as the reference and α-Fe_2O_3 as working electrode. The 1 M NaOH was used as an aqueous electrolyte. The Electrochemical Impedance Spectra (EIS) measurement was recorded under illumination and darkness.

21.3 Results and Discussion

21.3.1 Structural and Phase Analysis

The structure and phase of the films was analyzed using x-ray diffraction (XRD) and Raman spectroscopy. Figure 21.1a shows the XRD pattern of the α-Fe_2O_3 thin film. The presence of multiple numbers of peaks in XRD pattern suggests the polycrystalline nature of α-Fe_2O_3 film. As seen from the figure main diffraction peaks were observed at $2\theta \sim 24.2^o$, 33.2^o, 35.5^o, 54.5^o, 61.5^o and 64.1^o corresponding to (012), (104), (110), (116), (213) and (300) crystal orientations respectively [27, 28]. These peaks are in agreement with JCPDS data file # 33-0664 of α-Fe_2O_3 with hexagonal crystal structure. The * indicates the diffraction peaks obtained from FTO glass substrate. The lattice parameters are calculated from peaks a = 5.03 Å and c = 13.7 Å, which are in agreement with standard reported values

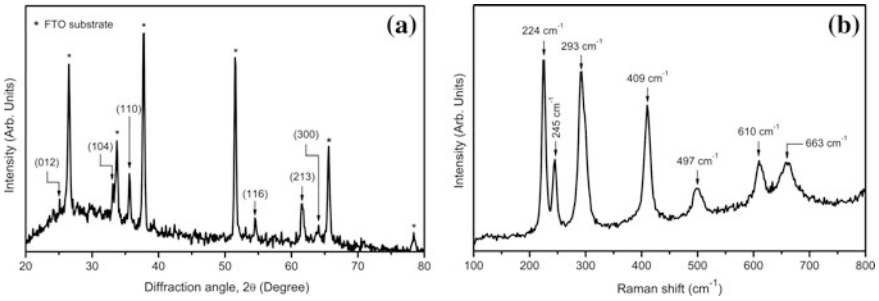

Fig. 21.1 **a** XRD pattern and **b** Raman spectra of α-Fe_2O_3 thin films electrodeposited on FTO substrate

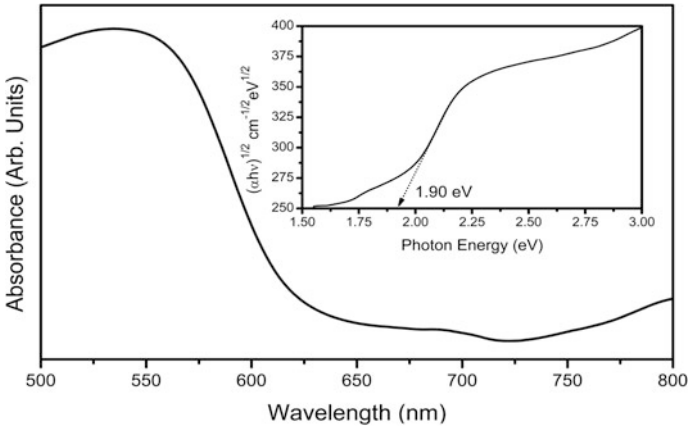

Fig. 21.2 UV-Visible absorbance spectra of α-Fe_2O_3 thin film. Inset shows Tauc's plot of α-Fe_2O_3 thin film used for estimation of band gap of α-Fe_2O_3 thin film

for α-Fe_2O_3 crystal structure. The crystallite domain size calculation was performed for the major diffraction peak (200) using the Scherrer's formula,

$$d_{x-ray} = \frac{0.9\,\lambda}{\beta \cos\theta_\beta} \tag{21.1}$$

where λ is the wavelength of the x-ray used, β is full-width at half-maximum (FWHM) and θ_β is the Bragg diffraction angle. The estimated average grain size using Scherrer's formula was found to be ~29 nm (Fig. 21.1a).

Raman spectroscopy is a powerful characterization tool to investigate molecular, vibration and chemical structure by interacting laser light with the sample. It is a non-destructive technique that offers a fast and simple way to determine the phase of the film. Figure 21.1b shows the Raman spectra of α-Fe_2O_3 thin film in the range 100–800 cm^{-1} deposited for 30 electrochemical cycles. As shown in figure major

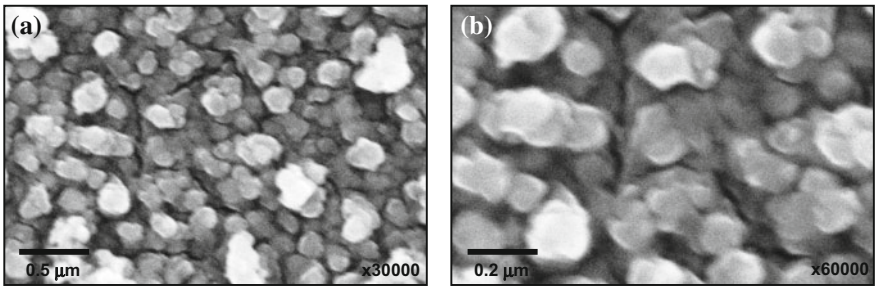

Fig. 21.3 Scanning electron microscopy images of electrodeposited α-Fe_2O_3 on FTO substrate at two different magnifications **a** At 30,000 and **b** At 60,000

Raman peaks were observed at ~224, 245, 293, 409, 497, 610 and 663 cm^{-1}. The Raman peaks located at ~224 and ~497 cm^{-1} corresponds to the A_1g mode whereas other peaks located at ~245, ~293, ~410, ~610 and 663 cm^{-1} corresponds to Eg mode of α-Fe_2O_3 [27, 28]. No other peaks were observed in the Raman spectra suggesting the formation of pure phase of α-Fe_2O_3.

21.3.2 Optical Analysis

In order to reveal the optical properties of the α-Fe_2O_3 thin films, UV-Visible spectroscopy has been used. Figure 21.2 shows the UV-Visible absorption spectra of α-Fe_2O_3 synthesized by electrodeposition. As seen the α-Fe_2O_3 exhibits a strong excitonic absorption around ~620 nm. Tauc relation was used to calculate the optical band gap (E_{opt}) of the electrodeposited α-Fe_2O_3 film [29],

$$(\alpha E)^{1/2} = B^{1/2}(E - E_{opt}) \tag{21.2}$$

where α is the absorption coefficient, B is the optical density of state and E is the photon energy. The optical band can be then calculated from a linear fit of the $(h\nu)^{1/2}$ versus hν plot (Tauc plot) [29]. Inset of Fig. 21.2 shows typical Tauc plot for the α-Fe_2O_3 thin film. The estimated value of optical band gap was found to be ~1.9 eV.

21.3.3 Surface Morphological Analysis

Scanning electron microscopy (SEM) was used to investigate the surface morphology of α-Fe_2O_3 thin film. Figure 21.3a, b show typical SEM micrographs of α-Fe_2O_3 thin film taken at two different magnifications. The surface of the films

shows granular morphology with uniform and dense growth of α-Fe_2O_3 on the FTO surface without having defects such as cracks, pinholes, and protrusion. The compositional analysis of the α-Fe_2O_3 thin film was carried out using energy dispersive x-ray analysis (EDAX) technique and found that Fe and O are approximately in the ratio of 2:3.

21.3.4 Photoelectrochemical (PEC) Measurements

The grown α-Fe_2O_3 thin films were used as working electrode (WE) in PEC cell. Electrochemical cell was used to conduct PEC performance, which was fitted with a water jacket around it, to prevent heating. Placed inside the cell were three electrodes; α-Fe_2O_3 thin film working electrode (WE), platinum foil counter electrode (CE), and saturated calomel reference electrode (SCE). 1 M NaOH was used as an aqueous electrolyte. Metrohm Autolab Potentiostat (PGSTAT302 N) and 150 W Xenon Lamp (PEC-L01) with 100 mW/cm^2 (AM 1.5) illumination intensity were used to record J-V characteristics, both under darkness and illumination.

To study the PEC performance of the synthesized α-Fe_2O_3 photoelectrodes we have performed electrochemical impedance spectroscopy (EIS) in a frequency range varying from 0.1 Hz to 100 kHz at a bias of 0 V versus SCE under UV-Visible light irradiation. The Nyquist diagram of EIS data is an effectual way to measure the electron transfer resistance. The arc radius in the Nyquist plot is directly related to electron transfer resistance reflecting energy barrier of the electrode reaction [30]. Figure 21.4a shows the EIS measurements using the Nyquist plot. The minimum of arc radius (∼25 Ω) shown in Fig. 21.4a reveals that there is large reduction in interfacial resistance between semiconductor and electrolyte due to the absorption of light and separation of electron-hole pairs away from interface. The photoelectrochemical (PEC) performance shown in Fig. 21.4b also supports this. The incident photon creates electron-hole pair when absorbed within photo electrode due to ejection of an electron from the valence band into the conduction

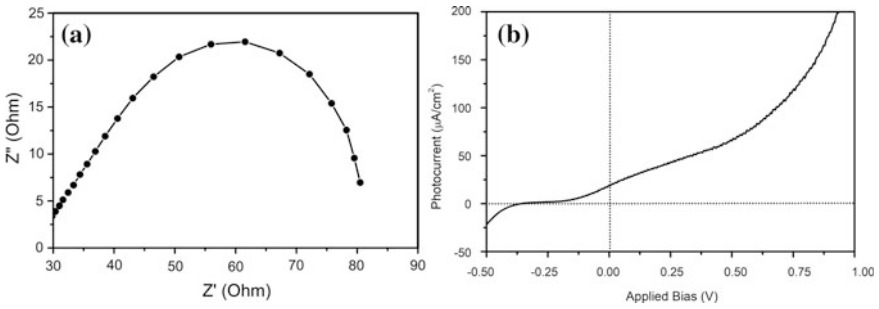

Fig. 21.4 **a** EIS Nyquist plot and **b** Photoelectrochemical (PEC) performance of α-Fe_2O_3 thin films electrodeposited on FTO substrate

band, leaving behind a hole in the valence band. The electron reduces the absorbed H^+ to produce H_2 and the hole oxidizes the OH^- ions to form stable OH [31]. In α-Fe_2O_3 it is difficult to separate photogenerated carriers due to the recombination loss and low diffusion length of charge carriers. However, in the present study an attempt has been made to obtain high photocurrent density with optimum film thickness. An excellent PEC performance for water splitting with higher photocurrent density ~65 μA/cm^2 at 0.5 V versus SCE under 100 mW/cm^2 illumination has been obtained.

21.4 Conclusions

In summary, hematite (α-Fe_2O_3) thin films photo-electrode were synthesized using a simple, controlled and cost effective electrodeposition technique for solar water splitting. Films were investigated using XRD, SEM, UV-Visible and Raman spectroscopy for their structural, optical and morphological properties. Further suitability of α-Fe_2O_3 thin films as a photo-electrode has been evaluated by photoelectrochemical (PEC) measurements with photocurrent density of 65 μA/cm^2 at 0.5 V versus SCE under AM 1.5 100 mW/cm^2 illumination. The absorption spectrum of α-Fe_2O_3 shows significant absorption in the visible region. However, photo-conversion efficiency is quite low. The obtained results suggest that a well controlled thick α-Fe_2O_3 material can be use as a shell layer with wide band gap nano-structured semiconductor like ZnO, TiO_2 to form hetero-structure for solar water splitting application. The effective enhancement in photocurrent conversion efficiency with optimum film thickness has been observed upon light irradiation.

References

1. J. Nowotny, C. Sorrell, L. Sheppard, T. Bak, Solar-hydrogen: environmentally safe fuel for the future. Int. J. Hydrogen Energy **30**(5), 521–544 (2005), doi:10.1016/j.ijhydene.2004.06.012
2. A. Fujishima, Electrochemical photolysis of water at a semiconductor electrode. Nature **238**, 37–38 (1972). doi:10.1038/238037a0
3. A. Kay, I. Cesar, M. Gratzel, New benchmark for water photooxidation by nanostructured -Fe2O3 films. J. Am. Chem. Soc. **128**(49), 15714–15721 (2006). doi:10.1021/ja064380l
4. F.L. Souza, K.P. Lopes, E. Longo, E.R. Leite, The influence of the film thickness of nanostructured -Fe2O3 on water photooxidation. Phys. Chem. Chem. Phys. **11**(8), 1215–1219 (2009). doi:10.1039/B811946E
5. J.H. Park, S. Kim, A.J. Bard, Novel carbon-doped TiO_2 nanotube arrays with high aspect ratios for efficient solar water splitting. Nano Lett. **6**(1), 24–28 (2006). doi:10.1021/nl051807y
6. D.K. Zhong, M. Cornuz, K. Sivula, M. Gratzel, D.R. Gamelin, Photo-assisted electrodeposition of cobalt- phosphate (Co-Pi) catalyst on hematite photoanodes for solar water oxidation. Energy Environ Sci **4**(5), 1759–1764 (2011), doi:10.1039/C1EE01034D

7. M. Chen, W. Li, X. Shen, G. Diao, Fabrication of core-shell α-fe$_2$o$_3$@ $Li_4Ti_5O_{12}$ composite and its application in the lithium ion batteries. ACS Appl. Mater. Interfaces. **6**(6), 4514–4523 (2014). doi:10.1021/am500294m
8. X. Zhu, Y. Zhu, S. Murali, M.D. Stoller, Nanostructured reduced graphene oxide/Fe_2O_3 composite as a high-performance anode material for lithium ion batteries. ACS Nano **5**(4), 3333–3338 (2011). doi:10.1021/nn200493r
9. Shao X. Zhao, Y. Zhang, X. Qian, Fe_2O_3/reduced graphene oxide/Fe_2O_3 composite in situ grown on Fe foil for high-performance supercapacitors. ACS Appl. Mater. Interfaces **8**(44), 30133–30142 (2016). doi:10.1021/acsami.6b09594
10. S. Jana, A. Mondal, Fabrication of SnO_2/α-Fe_2O_3, SnO_2/ α-Fe_2O_3-PB heterostructure thin films: Enhanced photodegradation and peroxide sensing. ACS Appl. Mater. Interfaces. **6**(18), 15832–15840 (2014). doi:10.1021/am5030879
11. J. Krysa, M. Zlamala, S. Kmentb, Z. Hubickab, Photo-electrochemical properties of wo3 and α-Fe2O3 thin films. Chem. Eng. Trans., 41 (2014) doi:10.3303/CET1441064
12. M. Niu, F. Huang, L. Cui, P. Huang, Y. Yu, Y. Wang, Hydrothermal synthesis, structural characteristics, and enhanced photocatalysis of sno$_2$/α-Fe_2O_3 semiconductor nanoheterostructures. ACS Nano **4**(2), 681–688 (2010). doi:10.1021/nn901119a
13. Z. Wei, R. Xing, X. Zhang, S. Liu, H. Yu, P. Li, Facile template-free fabrication of hollow nestlike α-Fe_2O_3 nanostructures for water treatment. ACS Appl. Mater. Interfaces. **5**(3), 598–604 (2012). doi:10.1021/am301950k
14. L.S. Zhong, J.S. Hu, H.P. Liang, W.G. Song, L.J. Wan, Self-assembled 3D flowerlike iron oxide nanostructures and their application in water treatment. Adv. Mater. **18**(18), 2426–2431 (2006). doi:10.1002/adma.200600504
15. K. Sivula, F.L. Formal, M. Gratzel, Solar water splitting: progress using hematite (α-Fe_2O_3) photoelec-trodes. Chem Sus Chem **4**(4), 432–449 (2011). doi:10.1002/cssc.201000416
16. A. Murphy, P. Barnes, L. Randeniya, I. Plumb, I. Grey, M. Horne, Efficiency of solar water splitting using semiconductor electrodes. Int. J. Hydrogen Energy **31**(14), 1999–2017 (2006). doi:10.1016/j.ijhydene.2006.01.014
17. A. Chai, J. Peng, B. Yan, Characterization of α-Fe_2O_3 thin films deposited by atmospheric pressure CVD onto alumina substrates. Sensors and Actuators B: Chemical **34**(1-3), 412–416 (1996). doi:10.1016/S0925-4005(97)80014-7
18. Y. Zhu, Y. Qian, M. Zhang, Z. Chen, D. Xu, L. Yang, Preparation and characterization of nanocrystalline powders of cuprous oxide by using ϒ-radiation. Mater. Res. Bull. **29**(4), 377–383 (1994). doi:10.1016/0025-5408(94)90070-1
19. S. Joshi, R. Nawathey, V. Koinkar, V. Godbole, S. Chaudhari, S. Ogale, S. Date, Pulsed laser deposition of iron oxide and ferrite films. J. Appl. Phys. **64**(10), 5647–5649 (1988). doi:10.1063/1.342258
20. S. Wilhelm, K. Yun, L. Ballenger, N. Hackerman, Semiconductor properties of iron oxide electrodes. J. Electrochem. Soc. **126**(3), 419–424 (1979). doi:10.1149/1.2129055
21. Q. Chen, Y. Qian, H. Qian, Z. Chen, W. Wu, Y. Zhang, Preparation and characterization of iron (iii) oxide (α-Fe_2O_3) thin films hydrothermally. Mater. Res. Bull. **30**(4), 443–446 (1995). doi:10.1016/0025-5408(95)00028-3
22. Y. Xie, W. Wang, Y. Qian, L. Yang, Z. Chen, Deposition and microstructural characterization of NiO thin films by a spray pyrolysis method. J. Cryst. Growth **167**(3-4), 656–659 (1996). doi:10.1016/0022-0248(96)00285-0
23. M. Mahadik, S. Shinde, V. Mohite, S. Kumbhar, A. Moholkar, J. Kim, C. Bhosale, Photoelectrocatalytic oxidation of rhodamine B with sprayed α-Fe_2O_3 photocatalyst. Mater. Express **3**(3), 247–255 (2013). doi:10.1166/mex.2013.1120
24. M.P. Dare-Edwards, J.B. Goodenough, A. Hamnett, P.R. Trevellick, Electrochemistry and photoelectro-chemistry of iron (III) oxide. J. Chem. Soc., Faraday Trans. 1 79/9:2027–2041 (1983) doi:10.1039/F19837902027
25. J.H. Kennedy, K.W. Frese, Photooxidation of water at α-Fe_2O_3 electrodes. J. Electrochem. Soc. **125**(5), 709–714 (1978). doi:10.1149/1.2131532

26. J. Krysa, M. Zlamal, S. Kment, M. Brunclikova, Z. Hubicka, TiO_2 and Fe_2O_3 films for photoelectrochemical water splitting. Molecules **20**(1), 1046–1058 (2015). doi:10.3390/molecules20011046
27. Q. Wei, Z. Zhang, Z. Li, Q. Zhou, Y. Zhu, Enhanced photocatalytic activity of porous α-Fe_2O_3 films prepared by rapid thermal oxidation. J. Phys. D Appl. Phys. **41**(20), 202002 (2008). doi:10.1088/0022-3727/41/20/202002
28. X. Hu, J.C. Yu, J. Gong, Fast production of self-assembled hierarchical α-Fe_2O_3 nanoarchitectures. J Phys Chem C **111**(30), 11180–11185 (2007). doi:10.1021/jp073073e
29. J. Tauc, A. Menth, States in the gap. J. Non-Cryst. Solids **8**, 569–585 (1972). doi:10.1016/0022-3093/72:90194-9
30. A. Mayabadi, A. Pawbake, S. Rondiya, A. Rokade, R. Waykar, A. Jadhavar, A. Date, V. Sharma, M. Prasad, H. Pathan, S. Jadkar, Synthesis, characterization, and photovoltaic properties of TiO_2/CdTe core-shell heterostructure for semiconductor-sensitized solar cells (SSSCs). J Solid State Electrochem, 1–12 (2016), doi:10.1007/s10008-016-3473-3
31. M.M. Ba-Abbad, M.S. Takri, A. Benamor, A.W. Mohammad, Size and shape controlled of α-Fe_2O_3 nanoparticles prepared via sol-gel technique and their photocatalytic activity. J Sol-Gel Sci. Technol **81**(3), 880–893 (2016). doi:10.1007/s10971-016-4228-4